Unwinding Dynamics of a Helically Wrapped Polymer

J.-C. Walter,[1,2,3] M. Baiesi,[4,5] E. Carlon,[6] and H. Schiessel[2]

[1] *Laboratoire Charles Coulomb UMR 5221, Université Montpellier 2 & CNRS, F-34095, Montpellier, France*
[2] *Instituut-Lorentz, Universiteit Leiden, P.O. Box 9506, 2300 RA Leiden, The Netherlands*
[3] *Institute for Theoretical Physics, KU Leuven, Celestijnenlaan 200D, Leuven, Belgium*
[4] *Dipartimento di Fisica e Astronomia, Università di Padova, Via Marzolo 8, Padova, Italy*
[5] *INFN, Sezione di Padova, Via Marzolo 8, Padova, Italy*
[6] *Institute for Theoretical Physics, KULeuven, Celestijnenlaan 200D, Leuven, Belgium*

(Dated: July 27, 2014)

We study the rotational dynamics of a flexible polymer initially wrapped around a rigid rod and unwinding from it. This dynamics is of interest in several problems in biology and constitutes a fundamental instance of polymer relaxation from a state of minimal entropy. We investigate the dynamics of several quantities such as the total and local winding angles and metric quantities. The results of simulations performed in two and three dimensions, with and without self-avoidance, are explained by a theory based on scaling arguments and on a balance between frictional and entropic forces. The early stage of the dynamics is particularly rich, being characterized by three coexisting phases.

PACS numbers:

I. INTRODUCTION

The genetic information in eukaryotic cells (including cells of animals and plants) is accessed through DNA unwinding on two different length scales. On the larger scale the DNA double helix has to unwind from proteins, on the smaller scale the two strands of the double helix need to be separated. In the first case a semiflexible polymer (DNA double helix) is wound almost two turns around a protein cylinder forming the so-called nucleosome [1, 2], in the second case two flexible polymers (chains of nucleotides) are twisted around each other leading to the much stiffer double helix. The unwinding of the DNA from the nucleosome or the separation of the DNA double helix is achieved inside a cell in various ways, often involving molecular motors (chromatin remodellers, polymerases...) that usually give access through a local opening of the structures. Inside a test tube unwinding can be induced, typically on a global scale, through a change in temperature (DNA melting/helix-coil transition [2–5]), salt concentration (salt-induced DNA release [6, 7]) or through application of an external force (nucleosome unwrapping [2, 8–11], DNA unzipping [4, 12]). Local unwinding can also occur spontaneously leading to the breathing of nucleosomes and of DNA (usually called site exposure in nucleosomes [2, 11, 13–15] and denaturation bubbles in DNA [2, 5, 16]). Finally, during transcription, where the elongating RNA polymerase produces a RNA transcript, one faces again the situation of a flexible chain, the transcript, being initially wound around the much stiffer DNA double helix [17].

To gain insights into the unwinding process it is convenient to start from simple setups. In this work we study the unwinding process of an idealized flexible polymer model that is initially wound around a stiff rod, in a configuration of minimal entropy, which resembles some of the features of the DNA or RNA unwinding. This model was introduced and studied in ref. [18]. Here we extend the results of that analysis focusing in particular on metric properties. We present a scaling argument which fully captures the early stages of the dynamics that is characterized by power-law scaling. Despite the simplicity of the model, there is a complex dynamical behavior.

It is the entropy gain that drives the polymer from the initial configuration toward the full random coil configuration. A sketch of this process is given in Figure 1, which shows different snapshots of the polymer configurations in the course of a simulation. The polymer is initially fully wound in a helix around the rigid rod. One end of the polymer is tethered to the rod whereas the other end is free, hence the relaxation proceeds from the free end. This process shares some similarities with the simpler problem of the relaxation from one end of a completely stretched polymer [19, 20]. Consider a polymer tethered at one end and fully stretched by a strong flow. When the flow is turned off the polymer relaxes back to its coiled equilibrium conformation. As one end is tethered the relaxation starts from a free end, from where the coil grows. The unwinding has a similar relaxation from the free end which occurs through a rotational motion instead of a translational recoiling. However, the phenomenology in the case of unwinding is much richer, as we will show.

This paper is organized as follows. In the section Models and Simulations, we review the models and the type of Monte Carlo simulations used. In the section Results and Discussion, we focus first on the early unwinding dynamics which is characterized by power-laws scaling in time. It is shown that force balance equations and scaling arguments yield exponents in very good agreement with simulations. Second, we discuss the late stage of the relaxation process. Here the theory of ref. [18] predicts a power-law scaling for the longest relaxation time with logarithmic corrections. The analysis is extended to

other lattice and off-lattice models and the results confirm the validity of the theory.

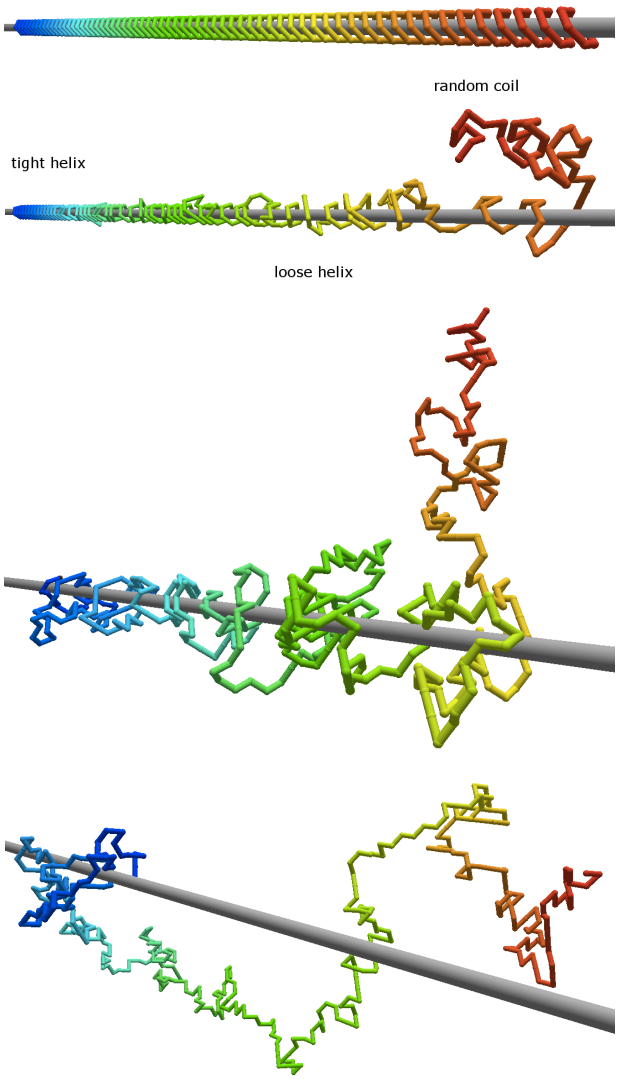

FIG. 1: Snapshots of a SAW with $L = 384$ monomers during unwinding from a rod. One end (blue) is attached to the rod and the other end (red) is free. Snapshots are taken at times $t = 0$, $t = 7 \times 10^4$, $t = 2 \times 10^6$, and $t = 5 \times 10^6$ (from top to bottom). The second configuration is in the early stage of the unwinding, where one can recognize three different phases: the part close to the fixed end is still a tightly wound helix, the middle section shows a loose helix configuration, and the part close to the free end forms a random coil.

II. MODELS AND SIMULATIONS

Figure 1 shows different snapshots of the polymer configurations during the unwinding from an infinitely long rod. Initially the polymer is fully wound and in the course of time it unwraps. The polymer has L monomers labeled with indices $1 \leq k \leq L$. One end ($k = 1$) is fixed to the rod, while the other end ($k = L$) is free. We have studied different cases to check the robustness and universality of the numerical results. For the ideal chain (the case without excluded volume) we modeled the polymer in three different ways. In a first model we considered a random walk (RW) with unit steps on a face-centered cubic (FCC) lattice. In the initial helical configuration, the polymer performs one turn in six steps along the rod. An update of the configuration consists of L attempts of so-called corner flips, where the randomly selected monomer is moved to a neighboring lattice site if the distances to the neighboring monomers are conserved (this is a lattice realization of Rouse dynamics [21]). The new configuration is accepted if the monomer does not overlap with the rod.

We also considered a random walk on a square lattice (i.e., a bidimensional lattice). In this case the starting configuration consists of a chain with a rescaled segment length wound around the origin. In the initial configuration on the square lattice one turn around the origin is performed by 8 monomers. The corner flip method is used here as well.

Finally, we used a freely jointed chain (FJC) to model three-dimensional off-lattice polymers. Neighboring monomers have a fixed distance a from each other and the rod has a diameter $1.5\,a$ ensuring that monomers cannot accidentally pass from one side to the other in the course of unwinding. The initial helical configuration is such that one turn is performed with 10 monomers. Also in this case a time step of the dynamics consists in L attempts of moves for randomly chosen monomers. When a monomer is selected, a new configuration is constructed via a rotation of that monomer around the axis defined by the two neighboring monomers by an angle randomly selected from $[0, 2\pi]$. The free end is updated with a new random position preserving the bond length with the second monomer. The new configuration is accepted if it does not overlap with the rod.

For the case of a polymer with excluded volume we use only the model of a self-avoiding walk (SAW) on the FCC lattice. The procedure is the same as for the ideal chain on the FCC lattice, with the added constraint of excluded volume between the monomers: one rejects moves violating it.

III. RESULTS AND DISCUSSION

A. Short-Time Dynamics

1. *Radial Distance*

We consider first the "radial" distance R_e which is defined as the average distance of the free end monomer from the rod. This quantity is shown in Figure 2 (RW's) and 3 (SAW). Starting from a minimal value for the fully wrapped configuration at $t = 0$ the growth of R_e follows a power law. In the ideal chain cases we find a first,

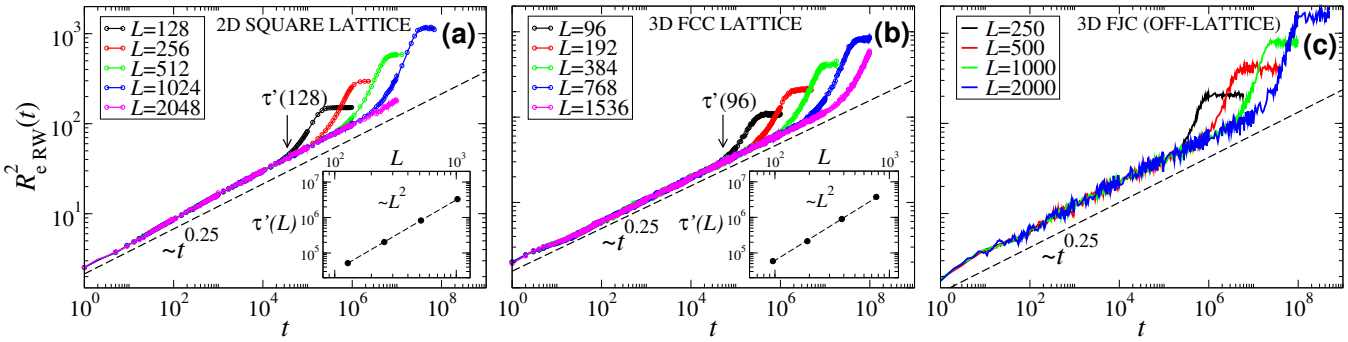

FIG. 2: Average squared distance $R^2_{\rm e\,RW}$ of the free end from the rod versus time (ideal chain) for (a) a 2D polymer on a square lattice, (b) a 3D polymer on a FCC lattice and (c) a FJC in 3D, for various chain lengths. For the three models the short time regime follows the power law $R^2_{\rm e\,RW} \sim t^{0.25}$. This regime ends at times scaling as $\tau' \sim L^2$, see insets (the values of τ' for the shortest chains are indicated by vertical arrows). The plateaus indicate the completion of relaxation. The averages are made at least (for the largest sizes) over (a) 2000 and (b) 3000 configurations. In (c), due to larger computational effort in continuous space for a local move, the average is performed only over 150 configurations, which explains the larger noise.

short-time, regime:

$$R^2_{\rm e\,RW}(t) \sim t^{0.25}\,. \tag{1}$$

This scaling with time of a spatial length scale is remarkably slow ($|R_{\rm e}| \sim t^{1/8}$) compared to the usual relaxation time scales encountered in polymer physics. The exponent is robust and is found in the minimalistic 2D polymer on a square lattice (Figure 2(a)), the RW on a FCC lattice (Figure 2(b)) and the freely jointed chain off-lattice (Figure 2(c)). We performed also simulations for a 3D excluded volume chain on an FCC lattice, for which we find a power law with a slightly larger exponent:

$$R^2_{\rm e\,SAW}(t) \sim t^{0.27}\,, \tag{2}$$

as it can be seen in Figure 3.

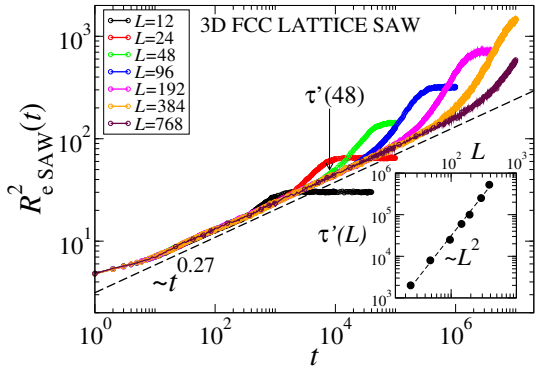

FIG. 3: Squared distance $R^2_{\rm e\,SAW}$ of the free end from the rod versus time for a excluded volume chain on an FCC lattice. The short time regime follows the power law $R^2_{\rm e\,SAW} \sim t^{0.27}$. The inset shows the scaling of τ' with the polymer length. Averages are made at least over 3000 configurations (for the largest size).

To understand the origin of this exponent we model the unwinding starting from a two phase picture. We assume that during the early stage of the dynamics the polymer starting from the fixed end has n monomers tightly wrapped around the rod, which are frozen as in their initial $t = 0$ configuration, while $L - n$ monomers are loose (we indicate these as phase 1 and phase 2, respectively, see Figure 4(a)). We assume that the loose monomers form a homogeneous helix with a constant pace, but which is loosely wrapped around the rod. Obviously, if the loose helix would extend until the free end of the polymer, the radial distance $R_{\rm e}$ would not grow in time. The two phase model is the starting point of our analysis and we will focus on the configuration of the polymer close to the free end later. We assume that the dynamics is governed by the following equation:

$$\gamma_2 \frac{dn}{dt} = -\frac{\partial \mathcal{F}}{\partial n}\,, \tag{3}$$

which is a balance between frictional and "entropic" forces during the growth of the helical domain. Here $\mathcal{F}(n) = f_1 n + f_2(L-n)$ is the total free energy of the configuration, with f_1 and f_2 the free energies per monomer of the two phases (with $f_2 < f_1$ as the loose helix has a higher entropy than the tight helix). γ_2 is the friction coefficient. The total winding angle of the last monomer is equal to 2π times the number of times the polymer is wrapped around the rod. For the two helices model such a quantity is then given by:

$$\Theta = n\Delta\theta_1 + (L-n)\Delta\theta_2\,, \tag{4}$$

where $\Delta\theta_1$ and $\Delta\theta_2$ are the densities of winding for the two phases (with $\Delta\theta_1 > \Delta\theta_2$, as phase 2 is more loosely wrapped compared to phase 1). A decrease in n leads to a decrease in the total winding angle and the whole loose helix rotates in a corkscrew motion. The friction coefficient is then proportional to the length of the rotating domain $\gamma_2 \sim (L-n)$. Using this input and the form of $\mathcal{F}(n)$ we get from the integration of eq. (3):

$$L - n \sim \sqrt{t}\,. \tag{5}$$

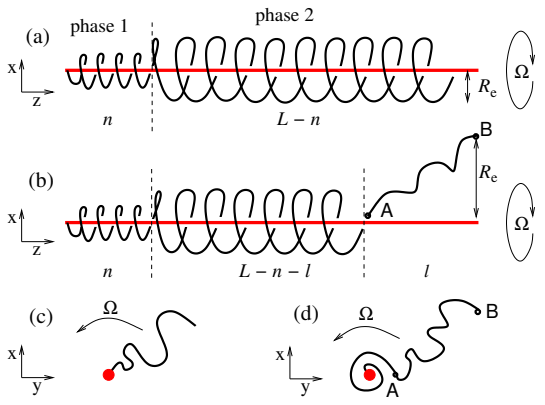

FIG. 4: (a-b) Configurations of the polymer during unwinding. (a) Two phase model consists of a tight helix (phase 1), which is the initial conformation, and a loose helix with constant pace (phase 2). (b) Extension of the two phase model accounting for the growth of an unwound coil of length l at the polymer end. (c-d) View of a polymer anchored to the rod (which is perpendicular to the plane) and rotating with angular velocity Ω. If Ω is small the polymer rotates while maintaining its equilibrium shape (case (c)). For high Ω the polymer gets partially wrapped around the rod, while a part of length l maintains its equilibrium shape. Equation (9) gives an estimate of the length l.

The angular velocity is given by eq. (4):

$$\Omega = \frac{d\Theta}{dt} \sim \frac{dn}{dt} \sim \frac{1}{\sqrt{t}}\,, \tag{6}$$

which decreases in time as there is an increasing friction when the loose helix grows.

The assumption that phase 2 is a helix of constant pace and radius is an approximation. However, as we will show, the numerical data are in good agreement with a square root growth (eq. (5)), which is a consequence of that assumption. Note that the assumption can be relaxed, allowing phase 2 to have fluctuations; the only essential requirement is that the friction γ_2 should scale linearly with the length of the domain. Our approximation is similar in spirit to the monoblock approximation where an inhomogeneously stretched polymer is modeled by a homogeneously stretched one, an approximation that does not change the scaling of the large scale geometry of the deformed chain [23, 24].

Let us consider now the growth of a coiled domain at the end of the chain (the stretch AB of length l shown in Figure 4(b)). This domain grows from a polymer rotating with angular velocity Ω. Let us assume that the friction originating from the coiled part is negligible compared to that of the loose helix, so the calculations leading to eqs. (5) and (6) remain valid. To understand the coil growth we consider a polymer attached to a rod and rotating with angular velocity Ω. If the polymer is sufficiently short and Ω small, its equilibrium conformation is not perturbed by the rotation and in particular it will have no winding (Figure 4(c)). If the polymer length exceeds a given threshold value, then part of the polymer close to the attachment point gets wound while the final part rotates maintaining its equilibrium shape (length of the part AB in Figure 4(d)). We estimate now the length of the end coil for a rotating polymer. To understand the calculation it is useful to consider the analogous problem of a polymer pulled by one end by a constant force [22, 23, 25–27]. The polymer maintains its equilibrium conformation if the applied force, f, or the polymer length, l, do not exceed the values fixed by the equation:

$$fR_F \sim k_B T\,, \tag{7}$$

where $R_F \sim l^\nu$ is the Flory radius, k_B the Boltzmann's constant and T the temperature. For a polymer rotating with an angular velocity Ω the force which distorts its shape is due to friction. The expression analogous to eq. (7) is then given by

$$\gamma v R_F \sim k_B T\,. \tag{8}$$

Using $v = \Omega R_F$ and $\gamma \sim l$ for a Rouse polymer we obtain the following relation for the length of the coiled unwound end of the rotating polymer:

$$l^{1+2\nu} \sim \frac{k_B T}{\Omega}. \tag{9}$$

Using the law (6) for the angular velocity we finally obtain for the growth of l:

$$l \sim t^{1/(4\nu+2)}\,, \tag{10}$$

and, from the equilibrium relation $R_e^2 \sim l^{2\nu}$ we find that the squared distance from the rod grows as:

$$R_e^2 \sim t^z\,, \tag{11}$$

with $z = \nu/(2\nu+1)$. Note that $z = 1/4$ for a Gaussian polymer ($\nu = 1/2$) and $z \simeq 0.27$ for a self-avoiding polymer ($\nu \simeq 0.59$) which is in excellent agreement with the numerical results (Figures 2 and 3).

We expect that the above description remains valid until the loose helix has grown to reach the first monomer. This corresponds to $n = 0$, i.e. when the tight helix has disappeared. According to eq. (5) this happens at a characteristic time τ' scaling as $\tau' \sim L^2$. We estimated τ' for polymers of different lengths from the simulation data of the radial distance of Figures 2 and 3. This is the time at which the growth law starts deviating from eq. (11). The vertical arrows in Figure 2 mark the estimated τ' for the polymer of shortest length. The insets of Figures 2(a) and (b) show plots of τ' vs. L as obtained from the data of the main plots. There is an excellent agreement with the predicted scaling $\tau' \sim L^2$. An equally good agreement was found for all the other cases studied. Note that the scaling $\tau' \sim L^2$ does not depend on the presence of self-avoidance, as demonstrated by the data in the inset of Figure 3.

We consider next the distance $d(s)$ between the free end monomer at position L and a monomer $L - s$ projected onto a plane perpendicular to the rod. In two

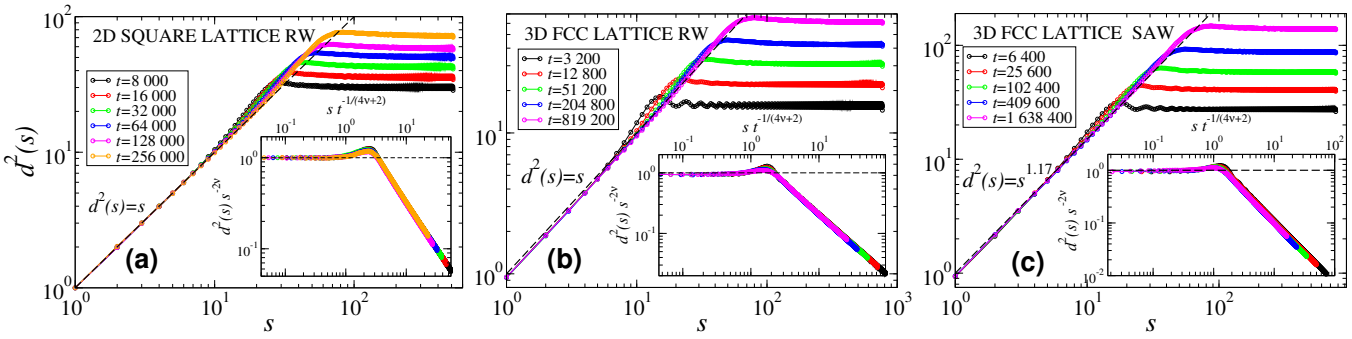

FIG. 5: Plot of $d^2(s)$ vs. s, for different times in the short time regime and $L = 768$. The quantity $d(s)$, defined in eq. (12), is the planar distance of the last monomer (index L) at the free end from the $(L - s)$-th monomer. For small s, one has $d^2(s) \sim s^{2\nu}$, indicating that the polymer forms a random coiled phase from its free end. The region where $d^2(s) \sim s^{2\nu}$ holds grows in time. The cases shown are (a) 2D RW, (b) RW on the FCC lattice, (c) SAW on the FCC lattice. The insets show rescalings of the data, see eq. (13).

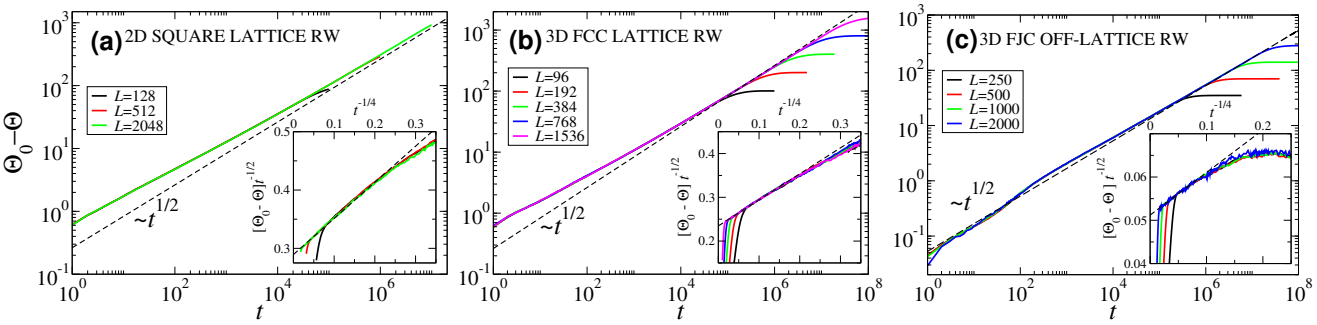

FIG. 6: Scaling of $\Theta_0 - \Theta$ vs. time, for different polymer lengths, for the ideal chain models. The numerics are well fitted by a power law $\sim t^{1/2}$. (Insets) Plots of $(\Theta_0 - \Theta)t^{-1/2}$ vs. $t^{-1/4}$. The dashed line is the slope predicted from eq. (15).

dimensional models this is equal to the total distance $d(s) \equiv |\vec{R}_L - \vec{R}_{L-s}|$ where $\vec{R}_i$ is the position of monomer i. In three dimensions, for a rod parallel to the z-axis we have:

$$d(s) = \sqrt{(x_L - x_{L-s})^2 + (y_L - y_{L-s})^2}\,, \qquad (12)$$

where x_i and y_i are the coordinates of the monomer i. In all cases analyzed (see Figure 5) we find for small s a scaling $d^2(s) \sim s^{2\nu}$ which demonstrates that the end part of the polymer is an equilibrated coil. The plots show that $d^2(s)$ saturates at a constant value for sufficiently large value of s. This point identifies the end of the coil and the beginning of the loose helical region. From scaling arguments we expect:

$$d^2(s) = s^{2\nu} g\left(\frac{s}{t^{1/(4\nu+2)}}\right)\,, \qquad (13)$$

where for small values of $x = s/t^{1/(4\nu+2)}$ the function $g(x)$ converges to a constant. For large x we expect $g(x) \sim 1/x^{2\nu}$ as $d^2(s)$ is independent of s, as the projected distance from the end monomer to the monomers in the helical domain cannot increase. The inset of Figure 5 shows a scaling plot of $d^2(s)s^{-2\nu}$ vs. $s/t^{1/(4\nu+2)}$ in full agreement with the scaling ansatz (13). This result supports the prediction that the coil growths according to eq. (10). Note that the scaling function has a maximum at the crossover between the two scaling regimes. The maximum is not very pronounced but indicates that the polymer, compared to an equilibrated coil, is slightly more stretched in the vicinity of the rod.

2. *Dynamics of the Total Winding Angle*

The theory developed in the previous section can be tested also on the dynamics of the total winding angle. Taking into account the presence of the coil of length l at the polymer end we need to modify eq. (4) with:

$$\Theta = n\Delta\theta_1 + (L - l - n)\Delta\theta_2\,, \qquad (14)$$

as the coil, which is of length l, does not contribute to the winding. We define with $\Theta_0 = L\Delta\theta_1$ the initial total winding angle. Combining eqs. (5), (10) and (14), we then get:

$$\begin{aligned}\Theta_0 - \Theta &= (L - n)(\Delta\theta_1 - \Delta\theta_2) + l\Delta\theta_2\,,\\ &= At^{1/2} + Bt^{1/(4\nu+2)}\,,\\ &= At^{1/2}\left(1 + \frac{B}{A}\frac{1}{t^{\nu/(2\nu+1)}}\right)\,, \qquad (15)\end{aligned}$$

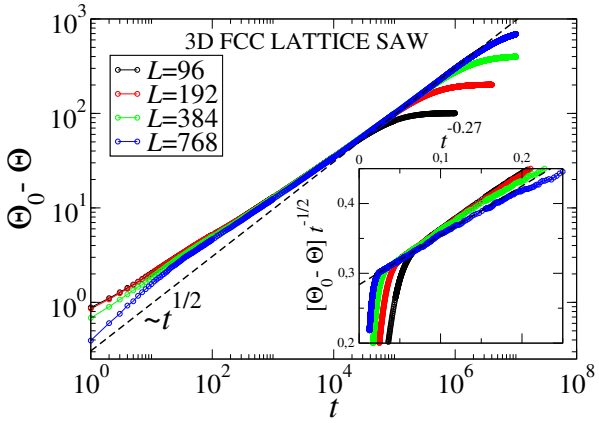

FIG. 7: Scaling of $\Theta_0 - \Theta$ vs. time, for different polymer lengths, for the SAW model. (Inset) Plot of $(\Theta_0 - \Theta)t^{-1/2}$ vs. $t^{-0.27}$. The dashed line is the slope predicted from eq. (15).

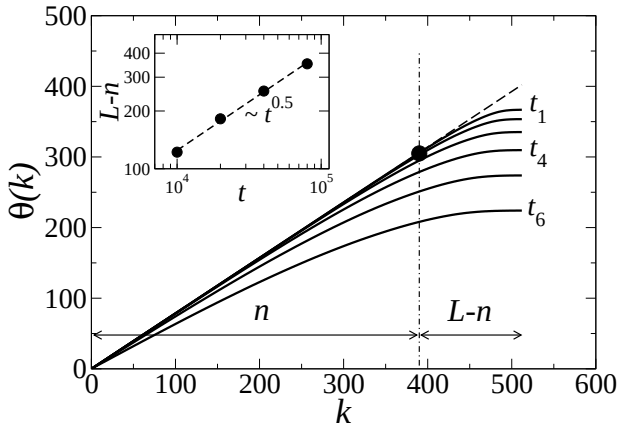

FIG. 8: Time evolution of the local winding angle $\theta(k)$ vs. monomer index k for the 2D RW of size $L = 512$. The dashed tilted line corresponds to the fully wrapped conformation $\theta(k) = \Delta\theta_1 k$. The data are obtained for increasing times $t_1 = 10\,000$, $t_2 = 20\,000$, $t_3 = 40\,000$, $t_4 = 80\,000$, $t_5 = 160\,000$ and $t_6 = 320\,000$. The vertical dashed-dotted line denotes the boundary between the tight helix of length n and the loose part of length $L - n$ at the time t_1. Inset: The growth of the loose domain follows the square root behavior predicted by eq. (5).

with A and B being some positive constants. The prediction is that $\Theta_0 - \Theta$ scales as $\sim \sqrt{t}$, with a slowly decaying correction term originating from the equilibrated end coil. The correction is predicted to scale as $\sim t^{-1/4}$ for a RW and $\sim t^{-0.27}$ for a SAW. In order to test the validity of eq. (15) we plot in Figure 6 the quantity $\Theta_0 - \Theta$ as a function of t in a log-log scale for three ideal-chain models in two and three dimensions, and the same for SAW's in Figure 7. In all cases the data approach for sufficiently long times the expected $\sim \sqrt{t}$ law.

To investigate the nature of the corrections to the leading scaling behavior we plot in the insets of Figure 6 the quantity $(\Theta_0 - \Theta)/\sqrt{t}$ vs. $t^{-\nu/(2\nu+1)}$. The data for short times and for different polymer lengths follow a straight line in good agreement with the prediction of eq. (15). The slope of the lines are positive and imply $B > 0$, as expected. Some stronger nonmonotonic behavior is observed in the 3D off-lattice model which does not have a counterpart in the other cases studied. The behavior of the winding angle was also investigated in a previous publication [18] and estimated to scale in the early time dynamics as $\Theta_0 - \Theta \sim t^{\rho}$ where $\rho \approx 0.43 - 0.44$. This seemed to match the short time dynamics rather well, although a closer inspection of the data shows that eq. (15) fits the data better. The analysis of the local winding, which follows, gives further support of a $\sqrt{t}$ growth of the unwound domain.

3. *Local winding angle*

Further insight of the polymer dynamics can be obtained from the analysis of the local winding angle $\theta(k)$, which is the winding angle of the k-th momomer. As the winding angle is counted from the monomer attached to the rod ($k = 1$) one has $\theta(1) = 0$, whereas the total winding angle defined above is $\Theta = \theta(L)$. Figure 8 shows the time evolution of $\theta(k)$ vs. k for different times and for a polymer of length $L = 512$ for a planar RW. At $t = 0$ the configuration is fully wrapped around the rod which corresponds to a linear increase $\theta(k) = \Delta\theta_1 k$. As the time evolves $\theta(k)$ decreases in a more pronounced manner starting from the free end of the polymer; at short times there is a domain of length n which is still fully wrapped as at time $t = 0$, followed by a loose part of length $L - n$. The inset of Figure 8 shows a plot of $L - n$ vs. t. The data are in very good agreement with the square root growth predicted by eq. (5). Differently from the data for the total winding angle of eq. (15), in this case there are no corrections to scaling expected.

B. Late Stage Relaxation

In the previous section we have fully characterized the early time relaxation dynamics. We found that the first regime in which the typical polymer configuration looks like in Figure 4(b) ends at a time scaling as $\tau' \sim L^2$. At very long times the dynamics was studied in ref. [18] using a force balance equation for the total winding angle Θ. This equation reads:

$$\gamma_\tau \frac{d\Theta}{dt} = -\frac{\partial \mathcal{F}}{\partial \Theta}\,, \tag{16}$$

where $\mathcal{F}$ is the free energy of a polymer in equilibrium with a total winding angle Θ and where $\gamma_\tau \sim L^{1+2\nu}$ is the friction coefficient. The free energy is a function of a scaling variable $\Theta/(\log L)^\alpha$, where α is an exponent governing the fluctuations of the winding angle at equilibrium. For RW's it is known rigorously [28] that $\alpha = 1$ while numerical simulations of 3D SAW's yield $\alpha \simeq 0.75$ [29].

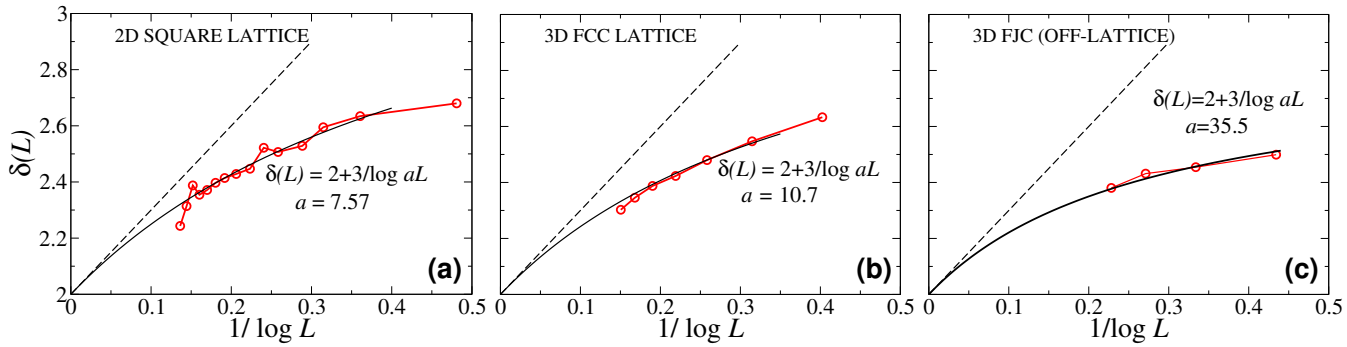

FIG. 9: Effective exponent defined by eq. (18) for models without self-avoidance in two and three dimensions. Asymptotically in L this quantity is expected to converge to $2\nu + 1 = 2$. The solid line is given by eq. (18) with a single adjustable parameter, the scale factor a.

For small winding angles the free energy is quadratic in the scaling variable, so that the relaxation to equilibrium becomes exponential [18]: $\Theta(t) \sim e^{-t/\tau}$ where τ is the longest relaxation time:

$$\tau \sim L^{2\nu+1} (\log L)^{2\alpha} . \qquad (17)$$

Since the initial configuration is fully wound with $\Theta_0 \sim L$, the total unwinding time is given by $\tau^* \sim \tau \log L$ [18]. The data are best analyzed using the definition of a running exponent, which probes the local slope of the data in a log-log plot. From eq. (17) we get:

$$\delta(L) \equiv \frac{d \log \tau^*}{d \log L} = 1 + 2\nu + \frac{2\alpha + 1}{\log(aL)} , \qquad (18)$$

where we have included a scale term a, in order to account for further corrections to scaling. Figure 9 shows a plot of the numerical value of $\delta(L)$ in two and three dimensions obtained from simulations of RW's. These data extend those of ref. [18] by including the three dimensional case for both FCC lattice (b) and off-lattice (c) models. The data are compared with eq. (18) where there is only a single adjustable parameter a used in the fit. The agreement is very good confirming the validity of the analytical approach of force balancing in eq. (16), which describes the process using the total winding angle as a single reaction coordinate.

IV. CONCLUSION

In this paper we have investigated the problem of the unwinding dynamics of a flexible polymer from a rigid rod. Scaling arguments and force balance equations allowed us to fully characterize the early stages of the unwinding and the late stages of the relaxation dynamics. These arguments are supported by extensive numerical simulations in two and three dimensions, with and without self-avoidance. The early dynamics can be understood by a three phase picture, where the polymer configuration starting from the fixed end can be described by a tight helix, a looser helix and a free random coil. The latter two phases grow in time following two different dynamical laws as predicted by eqs. (5) and (10). The analysis of various quantities from numerical simulations as metric distances or winding angles are all consistent with the analytical theory. Interestingly, the first growth law (5) does not contain the exponent ν and hence is superuniversal, being the same for random and self-avoiding walks. In the late stage dynamics we have extended the results of ref. [18] to different models and confirmed the scaling form of the longest relaxation time which involves logarithmic corrections.

The emerging picture is that of a relatively quick loosening of the polymer, which remains very close to the rod in the early stages of the dynamics. This is followed by an intermediate regime where the distance from the rod grows in a faster way and leads to the final relaxation. Differently from the early and late time behaviors the intermediate regime does not appear to display a clear cut scaling. This can be seen, for instance, in the behavior of R_e^2 depicted in Figure 2. During early dynamics, until a characteristic time τ', R_e^2 follows a power-law scaling. In the late time dynamics R_e^2 reaches a plateau. The intermediate time regime links the two regimes showing no clear evidence of a power law behavior. A typical snapshot of the intermediate regime is shown in Figure 1 (third configuration from the top). Its characterization remains a challenge for future work.

The two phase model description of polymer dynamics has recently gained some popularity: as examples we mention here the case of the translocation of a polymer through a nanopore [30–32], the pulling of a polymer by a constant force from one end [26, 27] and the folding of a DNA hairpin [33]. In these problems the polymer is subject to some local forcing and set into motion through the propagation of tension along its backbone. As the tension does not propagate instantaneously, the polymer is not set into motion at once. To describe the motion it is usually assumed that one can divide the polymer into different phases, which leads to some analytical predictions of the exponents governing the dynamics [30–33].

In this paper a similar approach was adopted to study a complementary case, namely that of the relaxation dynamics of an initially stretched (helically wrapped) polymer. The excellent agreement between simulations and model results shown in this paper, corroborates the validity of a two phase model approach in the description of nonequilibrium polymer dynamics.

Acknowledgement

We thank G.T. Barkema and A. Revyakin for stimulating discussions. This work is part of the research program of the Foundation for Fundamental Research on Matter (FOM), which is financially supported by The Netherlands Organisation for Scientific Research (NWO). J.-C.W. acknowledges the support by the Laboratory of Excellence Initiative (Labex) NUMEV, OD by the Scientific Council of the University of Montpellier 2 and HPC@LR for offering computational resources.

[1] Luger K., Mäder A.W., Richmond R.K., Sargent D.F. & Richmond T.J. (1997) Crystal structure of the nucleosome core particle at 2.8 Å resolution *Nature (London)* **389**, 251-260.

[2] Schiessel H. (2014) Biophysics for Beginners: a Journey through the Cell Nucleus (Pan Stanford Publishing, Singapore).

[3] Poland D. & Scheraga H.A. (1966) Occurrence of phase transition in nucleic acid models for gene regulation. *J. Mol. Biol.* **254**, 130-149.

[4] Kafri Y., Mukamel D. & Peliti L. (2002) Melting and unzipping of DNA *Eur. Phys. J. B* **27**, 135-146.

[5] Blossey R. & Carlon E. (2003) Reparametrizing the loop entropy weights: effect on DNA melting curves *Phys. Rev. E* **68**, 061911-1-8.

[6] Yager T.D., McMurray C.T. & van Holde K.E. (1989) Salt-induced release of DNA from nucleosome core particles *Biochemistry* **28**, 2271-2281.

[7] Kunze K.-K. & Netz R.R. (2000) Salt induced DNA-histone complexation *Phys. Rev. Lett.* **85**, 4389-4392.

[8] Brower-Toland B.D., Smith C.L., Yeh R.C., Lis J.T., Peterson C.L. & Wang M.D. (2002) Mechanical disruption of individual nucleosomes reveals a reversible multistage release of DNA *Proc. Natl. Acad. Sci. USA***99**, 1960-1965.

[9] Kulić I.M. & Schiessel H. (2004) DNA spools under tension *Phys. Rev. Lett.* **92**, 228101-1-4.

[10] Mihardja S., Spakowitz A.J., Zhang Y. & Bustamante C. (2006) Effect of force on mononucleosomal dynamics *Proc. Natl. Acad. Sci. USA***103**, 15871-15876.

[11] Blossey R. & Schiessel H. (2011) The dynamics of the nucleosome: thermal effects, external forces and ATP *FEBS Journal* **278**, 3619-3632.

[12] Essevaz-Roulet B., Bockelmann U. & Heslot F. (1997) Mechanical separation of complementary strands of DNA *Proc. Natl. Acad. Sci. USA* **94**, 11935-11940.

[13] Polach K.J. & Widom J. (1995) Mechanism of protein access to specific DNA sequences in chromatin: a dynamic equilibrium model for gene regulation *J. Mol. Biol.* **254**, 130-149.

[14] Koopmans W.J.A., Buning R., Schmidt T. & van Noort J. (2009) spFRET Using alternating excitation and FCS reveals progressive DNA unwrapping in nucleosomes *Biophys. J.* **97**, 195-204.

[15] Prinsen P. & Schiessel H. (2010) Nucleosome stability and accessibility of its DNA to proteins *Biochimie* **92**, 1722-1728.

[16] Ambjörnsson T., Banik S.K., Krichevsky O. & Metzler R. (2007) Breathing dynamics of heteropolymer DNA *Biophys. J.* **92**, 2674-2684.

[17] Belotserkovskii B.P. (2014) Relationships between the winding angle, the characteristic radius, and the torque for a long polymer chain wound around a cylinder: Implications for RNA winding around DNA during transcription *Phys. Rev. E* **89**, 022709

[18] Walter J.-C., Baiesi M., Barkema G. & Carlon E. (2013) Unwinding relaxation dynamics of polymers *Phys. Rev. Lett.* **110**, 068301-1-4.

[19] Brochard-Wyart F. (1995) Polymer chains under strong flows: stems and flowers *Europhys. Lett.* **30**, 387-392.

[20] Buguin A. & Brochard-Wyart F. (1996) Unwinding of Globular Polymers under Strong Flows *Macromolecules* **29**, 4937-4943.

[21] Doi M. & Edwards S. F. (1986) The theory of polymer dynamics (Oxford University Press, Oxford).

[22] Brochard-Wyart F. (1993) Deformations of one tethered chain in strong flows *Europhys. Lett.* **23** 105-111.

[23] Brochard-Wyart F., Hervet H. & Pincus P. (1993) Unwinding of polymer chains under forces or flows *Europhys. Lett.* **26** 511-516.

[24] Schiessel H. & Blumen A. (1997) Theory of dilute polyampholyte solutions in external electrical fields *Macromol. Theory Simul.* **6** 103-143.

[25] Schiessel H. & Blumen A. (1995) Fractal aspects in polymer science *Fractals* **3**, 483-490.

[26] Rowghanian P. & Grosberg A. Y. (2012) Propagation of tension along a polymer chain *Phys. Rev. E* **86** 011803-1-8.

[27] Sakaue T., Saito T. & Wada H. (2012) Dragging a polymer in a viscous fluid: Steady state and transient *Phys. Rev. E* **86** 011804-1-8.

[28] Rudnick J. & Hu Y. (1988) The winding angle distribution of an ordinary random walk *J. Phys. A: Math. Gen.* **20**, 4421.

[29] Walter J.-C., Barkema G. T. & Carlon E. (2011) The equilibrium winding angle of a polymer around a bar *J. Stat. Mech.* P10020.

[30] Sakaue T. (2007) Nonequilibrium dynamics of polymer translocation and straightening *Phys. Rev. E* **76** 021803-1-7.

[31] Rowghanian P. & Grosberg A. Y. (2011) Force-driven

polymer translocation through a nanopore: an old problem revisited *J. Phys. Chem. B* **115** 14127-14135.

[32] Sakaue T. (2011) Sucking genes into pores: Insight into driven translocation *Phys. Rev. E* **81** 041808-1-6.

[33] Frederickx R., in t'Veld T. & Carlon E. (2014) Anomalous Dynamics of DNA Hairpin Folding *Phys. Rev. Lett.* **112** 198102-1-5.